electronics

Article

MPC-ECMS Energy Management of Extended-Range Vehicles Based on LSTM Multi-Signal Speed Prediction

Laiwei Lu [1], Hong Zhao [1,*], Xiaotong Liu [1], Chuanlong Sun [1], Xinyang Zhang [2] and Haixu Yang [2]

1 College of Mechanical and Electrical Engineering, Qingdao University, Qingdao 266071, China; 2021023552@qdu.edu.cn (L.L.); 2020025567@qdu.edu.cn (X.L.); 2020020440@qdu.edu.cn (C.S.)
2 School of Mechanical Engineering, University of Science and Technology Beijing, Beijing 100083, China; m202120637@xs.ustb.edu.cn (X.Z.); haixuyang@xs.ustb.edu.cn (H.Y.)
* Correspondence: zhaohong@qdu.edu.cn

Abstract: Rule-based energy management strategies not only make little use of the efficient area of engines and generators but also need to perform better planning in the time domain. This paper proposed a multi-signal vehicle speed prediction model based on the long short-term memory (LSTM) network, improving the accuracy of vehicle speed prediction by considering multiple signals. First, various signals were collected by simulating the vehicle model, and a Pearson correlation analysis was performed on the collected multiple signals in order to improve the model's prediction accurate, and the appropriate signal was selected as the input to the prediction model. The experimental results indicate that the prediction method greatly improves the predictive effect compared with the support vector machine (SVM) vehicle speed prediction method. Secondly, the method was combined with the model predictive control-equivalent consumption strategy (MPC-ECMS) to form a control strategy suitable for power maintenance conditions enabling the equivalent factor to be adjusted adaptively in real-time and the target state of charge (SoC) value to be set. Pontryagin minimum principle (PMP) enables the battery to calculate the range extender output power at each moment. PMP, as the core algorithm of ECMS, is a common real-time optimal control algorithm. Then, taking into account the engine's operating characteristics, the calculated range extender power was filtered to make the engine run smoothly. Finally, hardware-in-the-loop simulation (HIL) was used to verify the model. The simulation results demonstrate that this method uses less fuel than the equivalent fuel consumption minimum strategy (ECMS) by 1.32%, 9.47% when compared to the power-following control strategy, 15.66% when compared to the SVM-MPC-ECMS, and only 3.58% different from the fuel consumption of the dynamic programming (DP) control algorithm. This shows that this energy management approach can significantly improve the overall vehicle fuel economy.

Keywords: extended-range bus; LSTM vehicle speed prediction; model prediction control (MPC); equivalent factor adaptive (ECMS)

Citation: Lu, L.; Zhao, H.; Liu, X.; Sun, C.; Zhang, X.; Yang, H. MPC-ECMS Energy Management of Extended-Range Vehicles Based on LSTM Multi-Signal Speed Prediction. *Electronics* **2023**, *12*, 2642. https://doi.org/10.3390/electronics12122642

Academic Editor: Carlos Andrés García-Vázquez

Received: 16 May 2023
Revised: 6 June 2023
Accepted: 7 June 2023
Published: 12 June 2023

1. Introduction

New energy vehicles have drawn more and more attention in recent years as energy and environmental issues have become more severe. Zhao et al. [1] studied the impact of unregulated emissions from fuel-powered cars on the environment and promoted Qingdao's "Oil-to-Gas" plan. Although pure electric vehicles have many advantages, such as low emissions and high efficiency, due to the limitations of small battery capacity, long charging time, and the small number of charging piles, the driving range of pure electric vehicles is short, which greatly affects the popularity of pure electric vehicles. Extended-range electric vehicle has become a research hotspot today because of a range extender that can continuously charge the battery, greatly increasing its driving range. The control strategy implements energy management by distributing power between the range extender and the power battery at various periods. In order to better distribute the range extender and battery output power, the rule-based control strategy was developed. Single-point and multi-point control are two rule-based control methods. Although the rule-based control strategy solves the problem of power allocation, it does not achieve optimal planning in most scenarios, so many scholars have proposed an optimization-based control strategy. The optimization-based control strategies, such as DP and PMP [2,3], adaptive equivalent fuel consumption minimum strategies (A-ECMS) [4], etc., typically optimize the original control strategy by using algorithms or calculate the global optimal control quantity from the global perspective.

Numerous academics have examined dynamic programming in recent years. Yuan et al. [5] designed a dynamic programming management strategy and applied it to automobiles, obtaining better experimental results and good vehicle economy. Zhang et al. [6] studied the control strategy for the optimal curve to improve the traditional power-following control strategy fuel economy. Chen et al. [7] designed a range-extender car using the DP control strategy. Pan et al. [8] applied the DP to supercapacitor hybrid electric vehicles for optimization, aiming to make the vehicle more economical. It is still difficult to achieve global optimization because of the uncertainty of future operating conditions. ECMS is a real-time control algorithm that changes from the Pontryagin minimum principle (PMP), which can equivalently convert electricity to fuel consumption by equivalent factors to calculate the control quantity and reduce fuel consumption. However, faced with constantly changing working conditions during driving, it is necessary to change the equivalent factor to maintain a constant SoC. Researchers have recently proposed more and more factor-adaptive approaches. Rezai et al. [9] proposed an ECMS strategy that adapts the equivalent factors according to the driving conditions. A hierarchical energy management strategy optimized in real time was proposed in [10], and heuristic DP was used to obtain optimal control and significantly improved fuel economy. Many researchers [11–13] adopted different speed prediction methods and combined MPC to optimize energy management strategies, such as the long short-term memory (LSTM), support vector machine(SVM), etc. Chen et al. [14] proposed an energy management method for driving condition recognition based on LSTM, which coordinated and optimized the engine speed according to different working conditions. Han et al. [15] studied the influence of electric motor (EM) thermodynamics on energy utilization efficiency based on vehicle speed prediction and MPC energy management. Lin et al. proposed an integrated-learning speed prediction-based energy management approach that considers adaptive reference SoC for driving modes [16].

Ritter et al. [17] proposed a novel method for successfully integrating long prediction ranges influenced by uncertainty in a stochastic MPC framework for hybrid electric car energy management. To increase the energy economy of metropolitan buses, Li et al. [18] proposed a control strategy that can manage energy based on driver behaviour types. A new driving pattern recognition method was designed to improve fuel economy and optimize power distribution by classifying the drive blocks by the K-means clustering algorithm [19]. An MPC based on an energy management strategy (EMS) and double-Q learning (DQL) was proposed for power distribution among multiple power sources in PHEVs [20]. Lin et al. [21] proposed an approach that can adjust the ECMS equivalent factor on time based on the unfinished mileage. The parameter identification method was used to identify the "black box" HEV model, and an EMS based on a two-layer MPC was proposed to optimize and control the operation process of HEV [22]. This method significantly reduced fuel consumption. Wang et al. [23,24] used improved control strategies to save fuel according to the driving patterns. Turker et al. [25] used neural networks for the energy management of cars, improving fuel economy. Al-Saadi et al. [26] improved vehicle economy by combining adaptive cruise control and MPC while ensuring safety. Wang et al. [27] proposed a power allocation strategy based on car operating conditions, driving mode prediction, and MPC, saving fuel while maintaining a constant SoC based on the tracking framework. Mu et al. [28] established a traffic flow statistical framework for long-term statistics, improving statistical efficiency and accuracy. Various random factors were considered to model the thermal runaway problem of overcharging batteries with multiple factors, and the reliability of this method was verified [29]. Hong et al. [30] established a new battery temperature prediction model through a new clustering data partitioning method and self-attention mechanism, providing accurate predictions throughout the seasons, reliably guaranteeing battery safety and greatly reducing the risk of battery runaway. Sun et al. [31] investigated LSTM speed prediction and improved MPC to improve the fuel economy.

Although many people have proposed MPC-EMS energy management strategies based on different neural network-structured vehicle speed prediction models, few studies have focused on the effect of multi-vehicle signals on speed prediction accuracy. Based on these studies, this paper proposes a combination of multiple signals LSTM prediction models and MPC-ECMS to adjust the fuel economy. The rest of this article is organized as follows. Section 2 introduces the optimal economic curve of the vehicle powertrain and the range extender. In Section 3, we carry out Pearson's correlation analysis of multiple signals during vehicle driving. Multiple signals are screened out to facilitate vehicle speed prediction, and the multi-signal LSTM vehicle and SVM vehicle velocity prediction are introduced. The predictive effects of the two methods and subsequently compared and analysed. Section 4 introduces the MPC-ECMS and compares the fuel consumption of various control strategies, including multi-signal-LSTM-MPC-ECMS, SVM-MPC-ECMS, DP-ECMS, and power-following control strategies.

The research in this paper provides a good reference for the energy management of various current models. In addition, this control strategy has good applicability to a wide range of vehicles. Multiple signal inputs can improve the accuracy of vehicle speed prediction, and the neural network has more support compared with a single signal. Furthermore, the prediction accuracy can be improved more effectively by using the LSTM memory function. Combining MPC with ECMS can effectively utilize the real-time performance of ECMS.

2. Powertrain Modelling

This article takes a four-wheel drive bus powered by a range extender and a battery as the research object; the engine and generator are mechanically connected to form the range extender. A DC/DC converter connects the battery and other power components, and the automotive structure used in this article is shown in Figure 1. The parameters of each major component are shown in Table 1.

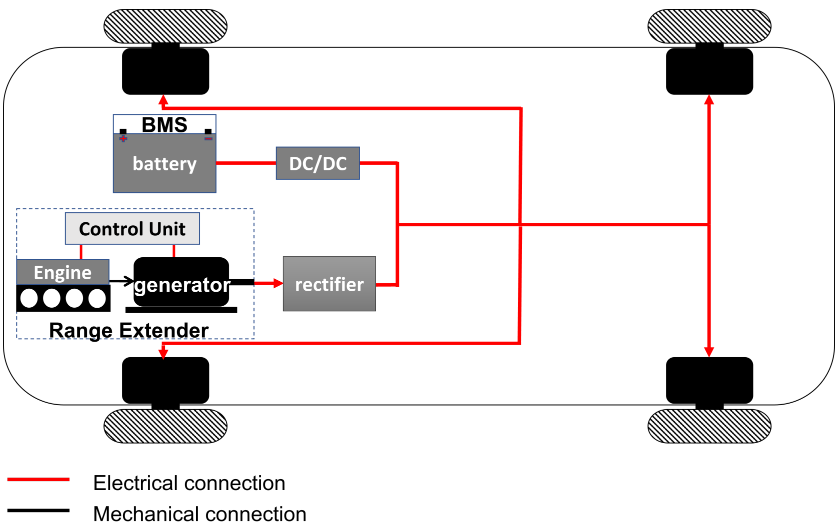

Figure 1. Range-extended vehicle structure.

Table 1. Main component parameters of range-extended vehicles.

Name	Parameters	Value	Parameters	Value
Vehicle	Total mass Aerodynamic drag coefficient	7000 kg 0.6	Wheel radius Front area	0.60 m 9 m^2
Engine	Engine type	Diesel engine	Maximum torque	2200 Nm
	Maximum speed	2000 r/min		
Electric motor	Maximum torque Type	1800 Nm Permanent magnet synchronous	Maximum speed	2650 r/min
Generator	Maximum torque	2200 Nm	Maximum speed	2000 r/min
Battery pack	Voltage	580 V	Capacity	200 Ah

2.1. Longitudinal Dynamics Model of the Vehicle

The longitudinal dynamics model is used to evaluate the performance of the vehicle under different operating conditions. It mainly considers the driving resistance according to the longitudinal dynamics principle of the whole vehicle; the driving resistance can be expressed by Equation (1)

$$F = Gf\cos\alpha + \frac{C_D A}{21.15}u^2 + G\sin\alpha + \delta m\frac{du}{dt} \tag{1}$$

where G is the gravity acting on the vehicle, N; α is the slope of the road; C_D is the air resistance coefficient; A is the windward area, m^2; δ is the rotational mass conversion factor; m is the mass, kg; and $\frac{du}{dt}$ is the driving acceleration, m/s^2.

2.2. Engine Model

The engine is the main power component of the model in this paper. In this study, the engine, generator and drive motor all adopt the quasi-static model. The quasi-static model is a simplified model that facilitates the description of static operating characteristics. The quasi-static model of the engine is shown in Figure 2. The quasi-static engine model demonstrate the changes in the engine fuel consumption rate with engine speed and torque, and is beneficial for the control strategy to find the optimal working state of the engine. The model can calculate the instantaneous fuel consumption in the following way:

$$m_f = T_{eng} \times n_{eng} \times be(T_{eng}, n_{eng}) \tag{2}$$

where m_f represents the engine fuel consumption rate, kg/h; T_{eng} is the engine torque, Nm; n_{eng} represents the speed, r/min; and be represents the equivalent fuel consumption rate, kg/KWh.

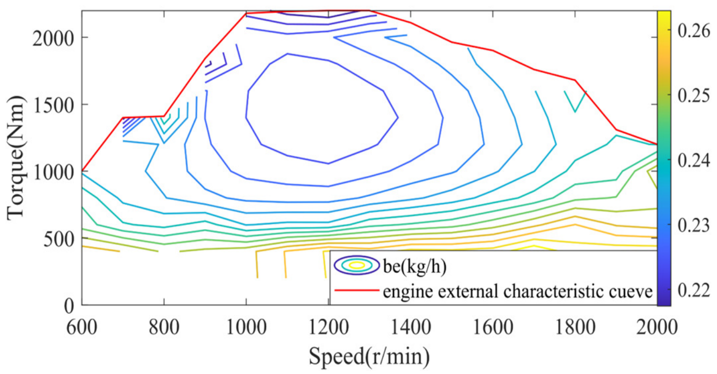

Figure 2. Engine BSFC.

2.3. Generator and Drive Motor Models

Generator and motor have similar characteristics and are used to achieve the conversion between mechanical and electrical energy. The quasi-static model of the generator and drive motor is shown in Figure 3. Because the generator and engine are mechanically connected, the optimal fuel consumption curve of the range-extender can be calculated by combining the drive generator and engine models. The optimal fuel consumption curve of the range-extender is shown in Figure 4a. The method for calculating the vehicle economy is as follows:

$$P_{Gen} = P_{eng}\eta(T_{eng}, n_{eng}) \tag{3}$$

$$feul_{eng} = f(T_{eng}, n_{eng}) \tag{4}$$

where P_{Gen} represents the generator output power; $\eta(T_{eng}, n_{eng})$ represents the generation efficiency, obtained according to the quasi-static model; P_{eng} represents the engine output power; $feul_{eng}$ represents the range-extender fuel consumption rate; T_{eng} represents the engine torque; and n_{eng} represents the engine speed.

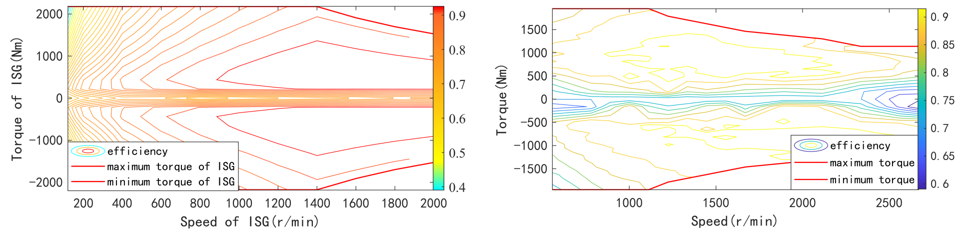

(**a**) (**b**)

Figure 3. Generator and motor efficiency. (**a**) Generator efficiency; (**b**) motor efficiency.

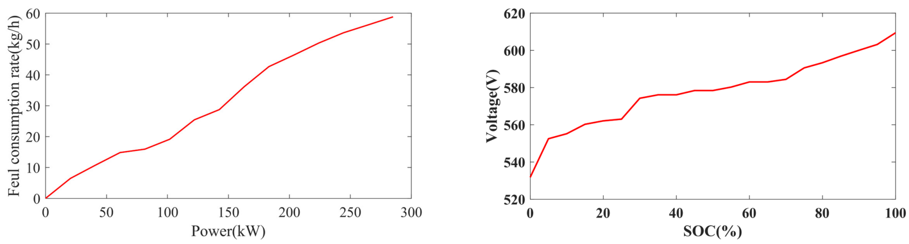

(**a**) (**b**)

Figure 4. Range-extender optimal fuel consumption curve and battery open circuit voltage. (**a**) Range-extender optimal fuel consumption curve; (**b**) battery open circuit voltage.

2.4. Power Battery Model

Using a battery as the energy storage element is an essential component of electric vehicles. The battery pack model adopts an equivalent circuit model, meaning the battery is equivalent to a voltage source and resistance. The voltage varies with the SoC, as shown in Figure 4b.

The modelling principle of power batteries is expressed as follows:

$$\mathrm{I(t)} = \frac{\mathrm{U_{VOC}}}{2\mathrm{R}} - \sqrt{\frac{\mathrm{U_{VOC}}^2}{2\mathrm{R}^2}\frac{\mathrm{P_b}}{\mathrm{R}}} \tag{5}$$

$$SOC(t) = SOC_{\text{init}} + \int_{t_0}^{t} \frac{U_{\text{VOC}} - \sqrt{U_{\text{VOC}}^2 - 4RP_b}}{2RQ} dt \tag{6}$$

where SOC_{init} represents the initial SoC value; U_{voc} represents the battery open circuit voltage; R represents the internal resistance; P_b represents output power; and Q represents the capacity.

The SoC and current are also within the battery's tolerance range.

3. Speed Prediction

This paper first collects various vehicle signals through simulation, then conducts Pearson's correlation analysis to select four signals with high correlation in the historical horizon, combined with vehicle speed to form the input layer data. Then, we input different signals in the historical time domain into the trained model to predict the vehicle speed. Finally, we propose a control strategy combining the MPC and ECMS to obtain adaptable equivalent factors and control quantities in the control time domain. The combination of MPC and ECMS enables real-time adjustment of the range-extender output power while facilitating short-term planning. In this section, we compare two machine learning-based prediction methods: (1) vehicle speed prediction by multi-signal LSTM; (2) vehicle speed prediction based on SVM. The test set adopts world transient vehicle cycle (WTVC), while the training set consists of six working conditions: NEDC, WLTC, UDDS, HEFET, FTP75, and EUDC. The speed changes in the training set are shown in Figure 5. The workflow of this study is shown in Figure 6.

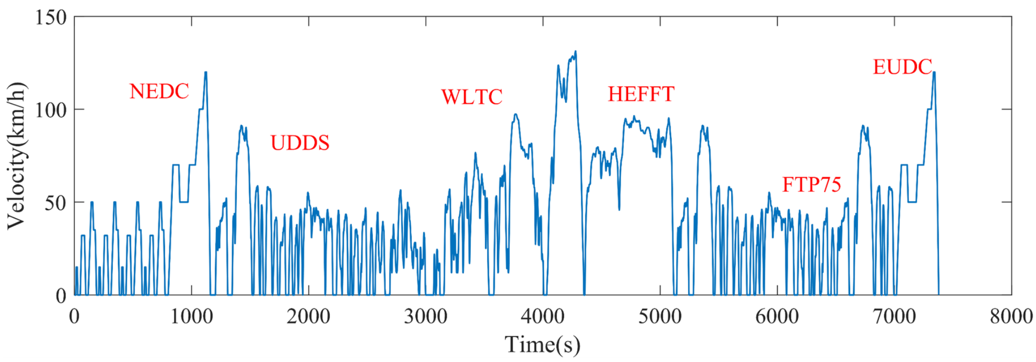

Figure 5. Vehicle speed prediction training set data.

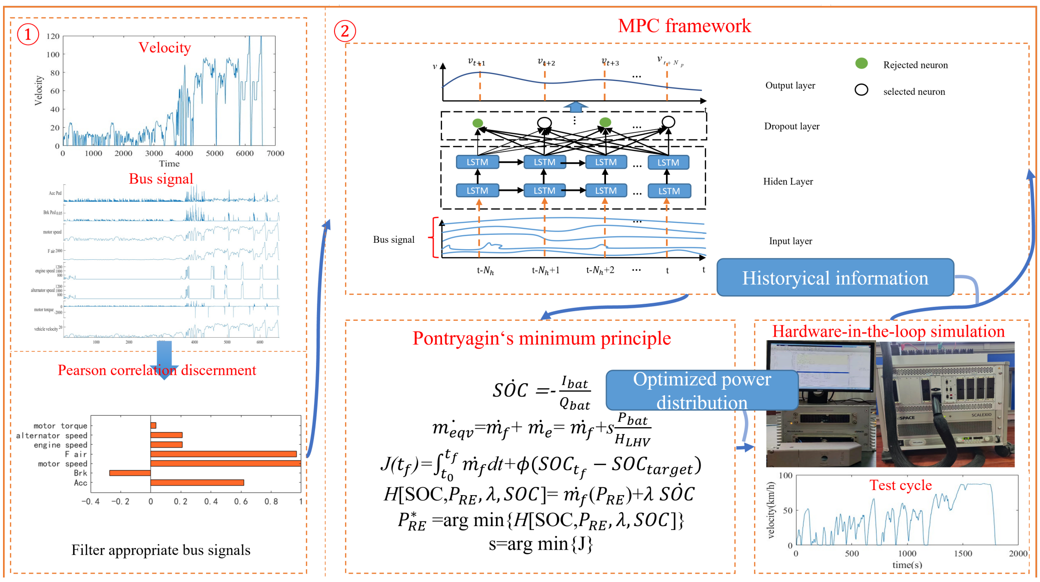

Figure 6. Flow chart of the velocity forecasting and energy management research.

3.1. Data Processing Based on Pearson's Correlation

In this paper, each vehicle signal is detected by simulation, and the correlation analysis is carried out with vehicle speed. Finally, four signals are selected together with the speed in the historical time domain to form the input data of the prediction model. The Pearson's correlation was developed by the British statistician Carl Smith and proposed by Pearson in the 20th century. The calculation formula for Pearson's correlation coefficient is as follows:

$$\rho_{X,Y} = \frac{\mathrm{cov}(X,Y)}{\sigma_X \sigma_Y} = \frac{E[(X-\mu_X)(Y-\mu_Y)]}{\sigma_X \sigma_Y} \tag{7}$$

where $\rho_{X,Y}$ is Pearson's correlation coefficient, representing the bus signal and vehicle speed; cov represents the covariance; σ indicates the standard deviation; E denotes the expectation; X represents each bus signal; and Y represents the actual vehicle speed. Table 2 shows the correlation coefficients between different bus signals and the actual speed.

Table 2. Pearson's correlation coefficients of each vehicle signal.

CAN Bus Signal	Pearson's Correlation Coefficient
Accelerator pedal opening	0.6192
Brake pedal opening	−0.2737
Motor speed	1
Air resistance	0.9687
Engine speed	0.2085
Alternator speed	0.2085
Motor torque	0.0356

According to Table 2, the accelerator pedal position, brake pedal position, motor speed, air resistance, and vehicle velocity are used as inputs for velocity prediction in the prediction domain.

3.2. Vehicle Speed Prediction Based on SVM

SVM is a machine learning algorithm commonly used for classification, which is extended to support vector regression (SVR) when applied to regression problems. SVR is a regression algorithm based on SVM, which can handle non-linear data and is usually used for time-series prediction. The process of SVR speed prediction is to collect the vehicle speed in the past n seconds to form the input and take the future speed in m seconds as the output. Figure 7 is a schematic diagram of the SVR to solve the linear regression problem. In the figure, the white circles indicate the vehicle speed in the past time, and the red circles indicate the vehicle speed predicted by the model.

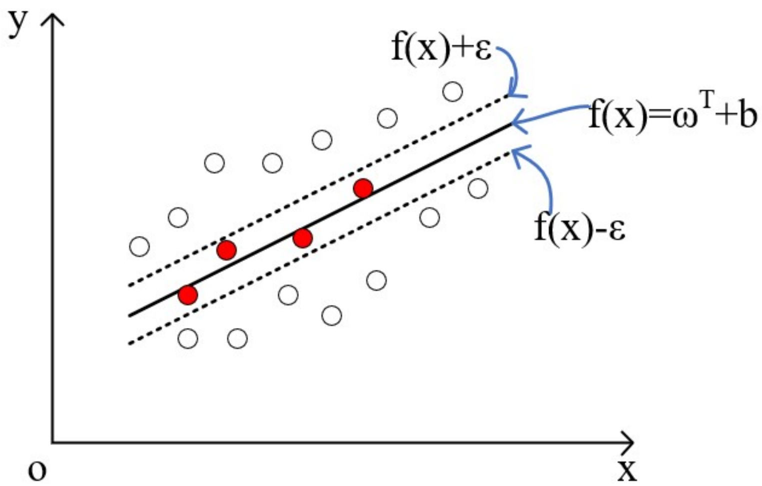

Figure 7. Schematic diagram of the support vector regression.

In contrast to traditional regression models, SVR assumes a minimum value ϵ exists such that ϵ is greater than or equal to the absolute difference between any predicted value $f(x)$ and the actual value y. Losses are calculated when the absolute value of

$y - f(x)$ exceeds ϵ, and the prediction is considered accurate when the absolute value of the difference from y is less than ϵ. Equations (8) and (9) show the expression of SVR and the loss function.

$$\min_{\omega,b} = \frac{1}{2}\|\omega\|^2 + C\sum_{j=1}^{m} l_\varepsilon(f(x_j) - y_j) \tag{8}$$

$$l_\varepsilon(z) = \begin{cases} 0, & if|z| \le \varepsilon; \\ |z| - \varepsilon, & otherwise; \end{cases} \tag{9}$$

where ω represents the normal vector; b represents the threshold; C represents the penalty parameter; and $ł_{epsilon}$ represents the insensitive loss of ϵ.

The slack variables ξ_j and $\xi_j{}^*$ are introduced and used to rewrite Equation (9), as shown in Equation (10).

$$\begin{array}{l} \min\limits_{\omega,b,\xi_j,\xi_j{}^*} \frac{1}{2}\|\omega\|^2 + C\sum\limits_{j=1}^{m}(\xi_j + \xi_j{}^*) \\ s.t. f(x_j) - y_j \le \varepsilon + \xi_j, \\ \quad y_j - f(x_j) \le \varepsilon + \xi_j{}^*, \\ \quad \xi_j, \xi_j{}^* \ge 0, j = 1, 2, \cdots, m \end{array} \tag{10}$$

The Lagrange multiplier is introduced to the original problem $\alpha_i, \alpha_i{}^*, \mu_i, \mu_i{}^*$ to construct the Lagrange function in Equation (11).

$$\begin{array}{r} L(\omega, b, \alpha, \alpha^*, \mu, \mu^*, \xi, \xi^*) = \frac{1}{2}\|\omega\|^2 + C\sum\limits_{j=1}^{m}(\xi_j + \xi_j{}^*) - \sum\limits_{j=1}^{m}\mu_j\xi_j - \\ \sum\limits_{j=1}^{m}\mu_j{}^*\xi_j{}^* + \sum\limits_{j=1}^{m}\alpha_j(f(x_j) - y_j - \varepsilon - \xi_j) + \sum\limits_{j=1}^{m}\alpha_j{}^*(f(x_j) - y_j - \varepsilon - \xi_j{}^*) \end{array} \tag{11}$$

Then, according to the dual condition and the KKT condition, the dual SVR problem is shown in Equation (12).

$$\begin{array}{c} \max\limits_{\alpha,\alpha^*} \sum\limits_{j=1}^{m} y_j(\alpha_j{}^* - \alpha_j) - \varepsilon(\alpha_j{}^* + \alpha_j) - \frac{1}{2}\sum\limits_{j=1}^{m}\sum\limits_{j=1}^{m}(\alpha_i{}^* - \alpha_j)(\alpha_j{}^* - \alpha_j)x_i{}^T x_j \\ s.t. \sum\limits_{j=1}^{m}(\alpha_j{}^* - \alpha_j) = 0, \\ 0 \le \alpha_j, \alpha_j{}^* \le C. \end{array} \tag{12}$$

Then, since the partial derivatives of ω, b,ξ_i and $\xi_i{}^*$ with respect to L are all 0, we obtain:

$$\omega = \sum_{j=1}^{m}(\alpha_j{}^* - \alpha_j)x_j \tag{13}$$

Then, the solution to the above regression problem is as follows:

$$f(x) = \sum_{i=1}^{m}(\alpha_i{}^* - \alpha_i)x_i{}^T x_i + b \tag{14}$$

where x is then mapped to a feature vector representation in a high-dimensional space, denoted as $\phi(x)$, and then introduced to the kernel function. The above equation can be represented as:

$$f(x) = \sum_{j=1}^{m}(\alpha_j{}^* - \alpha_j)\kappa(x, x_i) + b \tag{15}$$

The kernel function used in this article is the Gaussian radial basis function, as shown in Equation (16):

$$\kappa(x, x_j) = \exp(-g\|x - x_j\|^2) \tag{16}$$

From the above derivation, we know that the penalty factor C and kernel function bandwidth g directly impact the accuracy of the SVM speed predictions. The forecast accuracy can be increased by choosing the right C and g values.

The process of using SVR to solve the vehicle speed prediction problem is shown in Figure 8.In the figure, the arrows indicate that as time changes, '...' indicates the sliding window cycle calculation. It adopts a rolling prediction method to advance every second, using the vehicle speed in the historical time domain h as the input for the prediction model. The model operates and outputs the predicted velocity for the following p seconds, continuously updated throughout cyclic prediction.

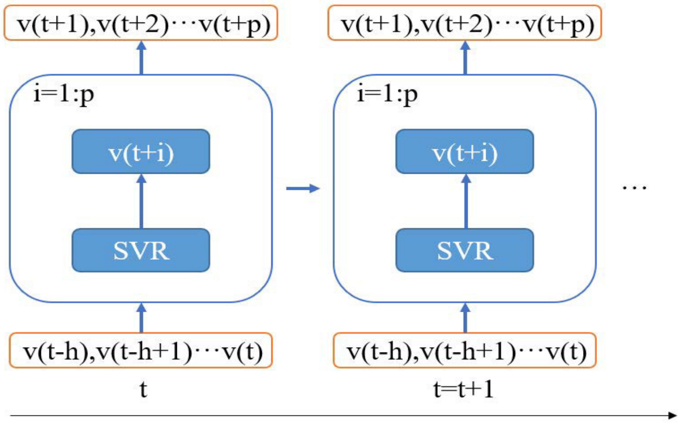

Figure 8. SVR speed prediction flowchart.

3.3. Multi-Signal Vehicle Speed Prediction Based on LSTM

Compared to a normal RNN, LSTM has a more extended short-term memory function. The key components of the LSTM are the memory unit and gate, and the input–output gate adjusts the content of the memory unit. Because of the gate structure, LSTM can avoid the "gradient disappearing" issue that plagues most RNN models. Information can be retained and gradients can be transferred over multiple time steps.

Figure 9 depicts the LSTM network configuration. The LSTM includes a unit state C compared to the RNN to save the long-term state. The input of an LSTM consists of three components: x_t, h_{t-1}, and C_{t-1}. Here, x_t represents the current input value, while h_{t-1} and C_{t-1} represent the output and state values from the previous time step, respectively. Two outputs are obtained through computation: the current output value h_t and the unit state C_t. Unlike traditional RNNs, LSTM uses three gates—input, output, and forget gates—to regulate the memory C. Retention of the input x_t in C_t is determined by the input gate, while the output gate determines how much of h_{t-1} and x_t is retained in h_t. The calculation formula for each parameter in the structure diagram is shown in Equation (17):

$$\begin{cases} f_t = \sigma(W_f[h_{t-1}, x_t] + b_f) \\ i_t = \sigma(W_i[h_{t-1}, x_t] + b_i) \\ g_t = \tanh(W_g[h_{t-1}, x_t] + b_g) \\ C_t = f_t \cdot C_{t-1} + i_t \cdot g_t \\ o_t = \tanh(W_o[h_{t-1}, x_t] + b_o) \\ h_t = o_t \cdot \tanh(C_t) \end{cases} \tag{17}$$

where f_t is the forget gate output value; i_t is the input gate output value; o_t is the output gate output value; σ represents the corresponding gate function; and W is the parameter of the gates.

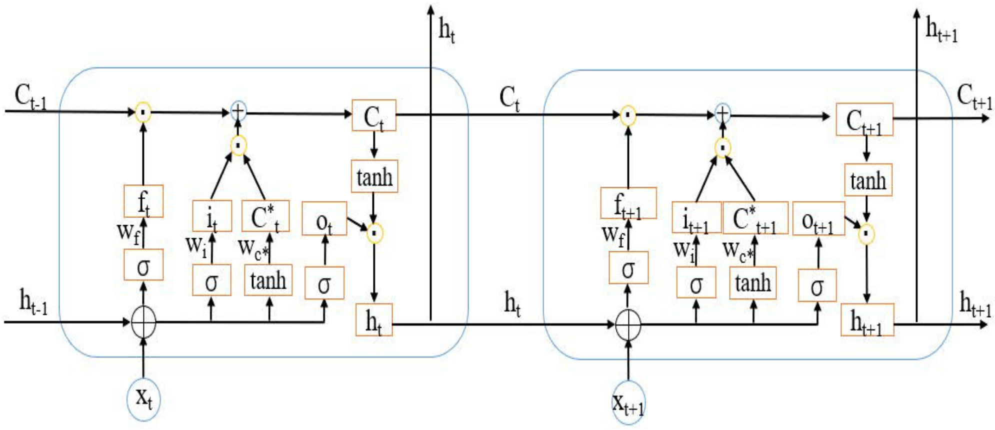

Figure 9. LSTM block diagram.

The process of predicting vehicle speed using LSTM is similar to the SVR method and is achieved through rolling prediction. As shown in Figure 10, N_h represents the historical temporal step size. By inputting the accelerator pedal opening, brake pedal opening, motor speed, air resistance, and historical vehicle speed information into the historical time domain, the neural network can calculate the change of speed within the subsequent p seconds. Then the rolling window is used for future speed prediction. During the training process, the network not only learns different features but also learns the noise in the training set which may cause the network to perform poorly on the test set due to overfitting. Therefore, this article adds a dropout layer. After adding the dropout layer, the neural network randomly deletes nodes in the hidden layer and all connections forward and backward with a probability p, thus forming a new network structure to ensure the model's generalization ability and prevent overfitting. This article uses a neural network with a dropout probability of 0.2, as shown in Figure 11. The green network nodes shown are the selected nodes, and the white nodes are abandoned nodes.

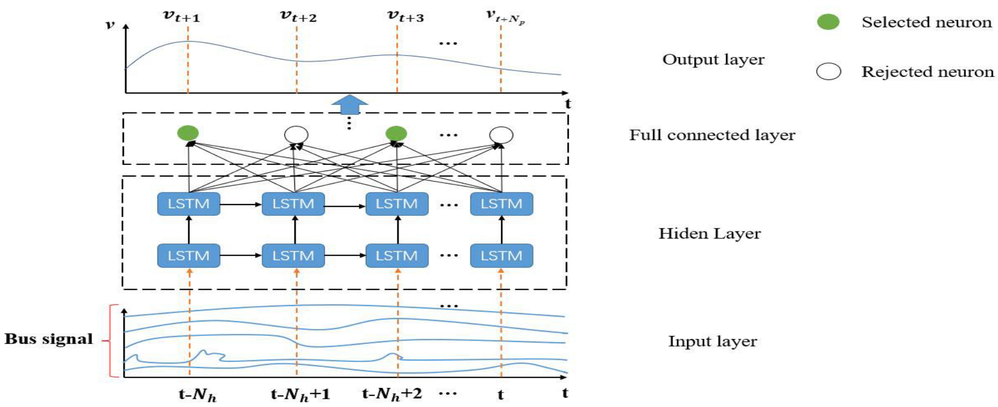

Figure 10. Multi-signal LSTM vehicle speed prediction schematic

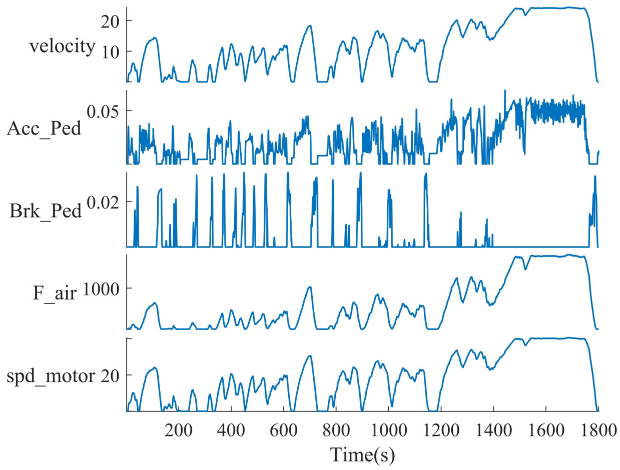

Figure 11. Multi-signal LSTM speed prediction input signal.

3.4. Vehicle Speed Prediction Results and Performance Comparison

We built a vehicle model and conducted a vehicle speed prediction simulation using Matlab2022b; the computer's CPU is Intel i7-9750H with a frequency of 2.60 GHz and 16 GB RAM. After the construction of two vehicle speed prediction models, both models were trained using the training set shown in Figure 6 and tested using the WTVC scenario as the test set. For the SVR model, only the speed with a historical time domain of 30 s was collected as prediction input. For the LSTM method, the historical vehicle speed, throttle pedal opening, brake pedal opening, and motor speed with a historical time domain of 30 s were collected for vehicle speed prediction inputs. Various vehicle signals collected from the whole vehicle model during the simulation of the training set are shown in Figure 11. When the historical time domain of both speed prediction methods was 30 s, and the prediction time domain was 5 s, the root mean square error (RMSE) of the multi-signal LSTM and SVR vehicle speed prediction methods were 3.0936 and 4.2482, respectively. The red part of the graph shows the predicted vehicle speed per second, and the black part shows the actual vehicle speed.The prediction results of the two methods are shown in Figure 12a. The performance of these two prediction methods under different prediction time domains while keeping the historical time domain at 30 s is shown in Table 3. It can be seen that the RMSE of the multi-signal LSTM speed prediction is smaller and more accurate, better reflecting the future trend of the vehicle speed. Therefore, we used the multi-signal LSTM to perform vehicle speed prediction and used the adaptive ECMS method as the energy management strategy based on the prediction. In this paper, the prediction time domain of 3, 5, and 7 s were performed to determine the most suitable prediction time domain size. The three vehicle speed prediction performances are shown in Figure 12b. We found that the larger the time domain of the prediction model, the relatively poorer the prediction accuracy. Additionally, considering the combination of energy management and vehicle speed prediction, it is not conducive to plan energy management strategies when the predicted future period is too short; therefore, 5 s was selected as the prediction time domain of the MPC framework for energy management so the MPC-ECMS could make optimal decisions.

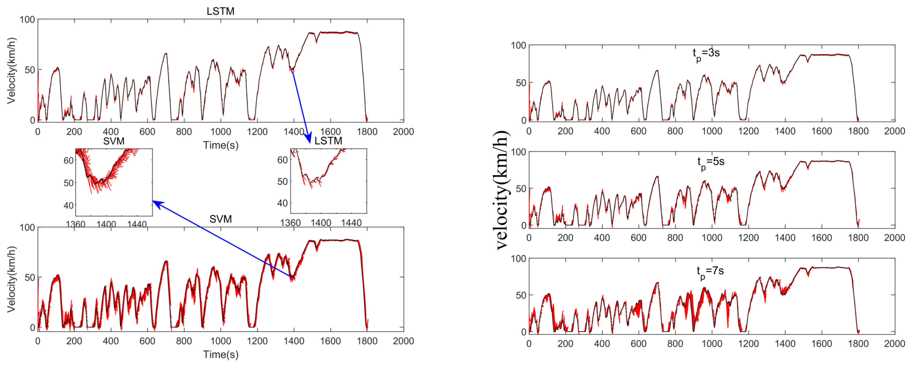

(**a**) (**b**)

Figure 12. Vehicle speed prediction effect of different prediction methods. (**a**) Comparison of multi-signal LSTM and SVM vehicle speed prediction; (**b**) comparison of multi-signal LSTM vehicle speed prediction in different prediction time domains.

Table 3. Performance comparison chart of the different vehicle speed prediction methods.

hp	**Multi-Signal LSTM**		**SVM**	
	T_pre **(s)**	**RMSE**	***T_pre*** **(s)**	**RMSE**
3 s	0.0044	1.6085	0.00611	2.3735
5 s	0.0034	3.0936	0.009597	4.2482
7 s	0.0045	6.6171	0.0234	6.9404

hp is the predicted time domain size, T_pre is the prediction time.

Further research on the two methods of speed prediction yielded SVM and multi-signal LSTM speed prediction heat maps, as shown in Figure 13. The experimental results show that when the prediction time was 3 and 5 s, the speed point distribution predicted by the multi-signal LSTM method is more concentrated around the true value than the SVM method and has a better predictive performance. When the prediction time was 7 s, although there are a few scattered points in the LSTM method, most of them are still concentrated around the true value. The results in Table 3 show that when the prediction time was 7 s, the predictive performance of the two methods is relatively similar.

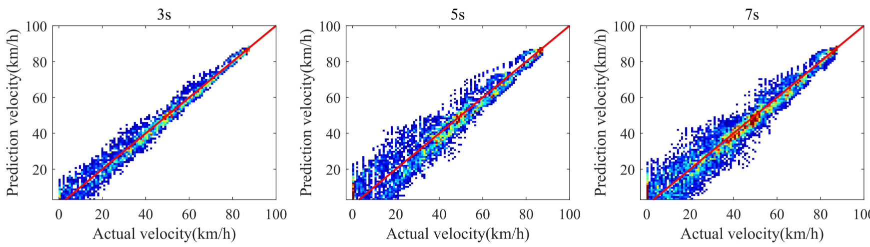

(**a**)

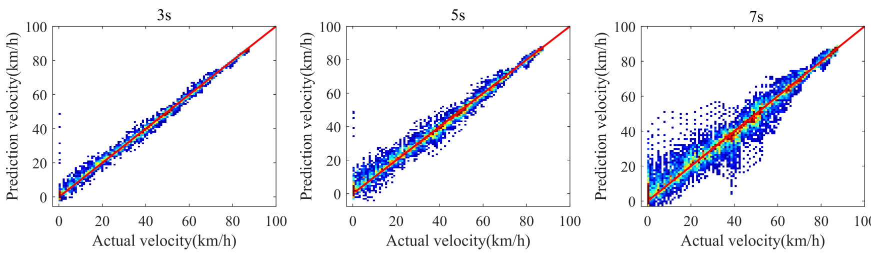

(**b**)

Figure 13. Vehicle speed prediction effect of the different prediction methods. (**a**) SVM speed forecast heat map comparison; (**b**) multi-signal LSTM speed prediction heat map comparison.

4. MPC-ECMS

The MPC-ECMS control strategy can use MPC to combine the speed prediction module and energy management module, achieving more accurate control. Compared with traditional ECMS control strategies, the MPC-ECMS energy management strategy can continuously adjust the equivalent factor by rolling optimization, ensuring that the SoC can always be maintained near the target value and avoiding the problem of the battery not operating optimally due to the SoC being too high or too low, caused by the inability of traditional ECMS equivalent factors to be changed. The MPC-ESMS energy management strategy utilizes both the flexibility of MPC and the real-time nature of ECMS to achieve real-time control by continuously adjusting the equivalence factors.

4.1. Energy Management Based on ECMS

The main idea of ECMS is the Pontryagin minimum principle (PMP). The PMP was proposed and proven by the former Soviet mathematician Pontryagin. Compared with the classical variational calculus method in solving the optimal control problem, the PMP has a wider application and fewer constraints, and its core conclusion is that in the time interval $[t_0, t_f]$, for any admissible control variable $u(t)$, there exists an optimal control $u^*(t)$ that minimizes the Hamiltonian function H, i.e.:

$$H[x^*, u^*, \lambda^*, t] \leq H[x^*, u, \lambda^*, t] \tag{18}$$

Range-extended vehicles mainly have two operating modes: energy consumption mode and SoC maintenance mode. This article proposes an energy management method under the energy maintenance mode, and we take the minimum fuel consumption under the electricity maintenance mode as the optimization objective. The SoC is regarded as the state variable, and the power generated by the range-extender as the control variable, which can transform this problem into a minimum principle problem. Its performance metric expression is as follows:

$$J(t_f) = \int_{t_0}^{t_f} \dot{m_f}(P_{RE})dt + \phi(SOC_{t_f} - SOC_{t\arg et}) \tag{19}$$

where $\dot{m_f}$ represents the instantaneous fuel consumption, kg; P_{RE} represents the range-extender output power, kW; $SOC(t_f)$ represents the SoC at the terminal time,%; SOC_target is the target SoC of the battery during battery sustaining mode,%; and ϕ is the penalty factor that enables the SoC to stay near the target value.

The equation of state and Hamiltonian function for the ECMS problem are shown in Equation (20):

$$\begin{cases} S\dot{O}C(t) = f[x, u, t] = -\frac{I_{bat}}{Q_{bat}} \\ H[SOC, P_{RE}, \lambda, t] = \dot{m_f}(P_{RE}) + \lambda\, S\dot{O}C \end{cases} \tag{20}$$

According to the PMP, the optimal output power solution formula for the range-extender can be obtained from Equation (21):

$$P_{RE}{}^*(t) = \arg\min\{H[x, u, \lambda, t]\}, P_{RE} \in U_{RE} \tag{21}$$

The necessary condition for solving the optimal output power sequence in the PMP is:

$$\begin{cases} S\dot{O}C(t) = f[SOC^*(t), P_{RE}{}^*(t)] \\ \dot{\lambda}^*(t) = -\lambda^*(t)[\frac{\partial f(SOC^*(t), P_{RE}{}^*(t))}{\partial SOC}] \\ SOC^*(t_0) = SOC_0 \\ SOC^*(t_F) = SOC_{t\arg et} \end{cases} \tag{22}$$

where SOC_0 represents the initial SoC, %; SOC_{target} represents the target SoC, %; t_0 represents the starting time of the operating condition, s; and t_f represents the simulation termination time, s. It is also known that in a range-extended electric vehicle operating in battery maintenance mode, the variation of the SoC is very small, and both the voltage and resistance are considered constant; thus, λ can be treated as a constant value.

$$\dot{\lambda}^*(t) = 0 \tag{23}$$

Therefore, the co-state variable can be approximated as a constant in the power maintenance mode. In the power sustaining mode, ECMS assumes that the output power of the range-extender and battery are all from fuel, and the battery is regarded as a buffer device for energy transfer. The equivalent fuel consumption can be calculated using the following equation:

$$\underset{eqv}{\dot{m}} = \dot{m}_f + \dot{m}_e = \dot{m}_f + s\frac{P_{bat}}{H_{LHV}} \tag{24}$$

where m_{eqv} is the equivalent fuel consumption, kg; m_f represents the fuel consumption, kg; P_{bat} represents the battery output power, kW; H_{LHV} is the heating value of th eengine fuel, kJ/kg; and s denotes the equivalent factor, representing the degree of conversion from fuel to electrical energy.

Based on the above derivation, the expression of the Hamiltonian function in the ECMS strategy can be obtained as follows:

$$H[SOC(t), P_{RE}(t), \lambda(t), t] == \dot{m}_f(t) - \frac{\lambda(t)H_{HLV}}{\eta_{bat}^{sign(P_{RE})}Q_{bat}U_{oc}}\frac{P_{bat}(t)}{H_{LHV}} \tag{25}$$

where U_{OC} is the voltage, V; and $\eta_{bat}^{sign(P_{RE})}$ varies depending on the working state of the battery. The equivalent factor expressions for batteries under different operating states can be obtained from Equations (24) and (25) as follows:

$$\begin{cases} s = -\frac{H_{LHV}}{\eta_{bat}^{sign(P_{RE})}Q_{bat}U_{OC}}\lambda(t) \\ s_{chg} = \eta_{dis}^2 s_{dis} \end{cases} \tag{26}$$

where s_{dis} is the discharge equivalent factor; $s_c hg$ is the charging equivalent factor; and η_{dis} is the discharge efficiency.

The range-extender has different working states when different equivalent factors are selected. This paper sets the reference SoC for power maintenance to 0.3. Figure 14 is the comparison diagram of SoC maintenance and vehicle fuel consumption when different equivalent factors are selected. Figure 14 shows that when the equivalent factor $s = 2.5$, the SoC change is mostly stable. As the value of s increases, the vehicle tends to use more fuel and continuously charge the battery.

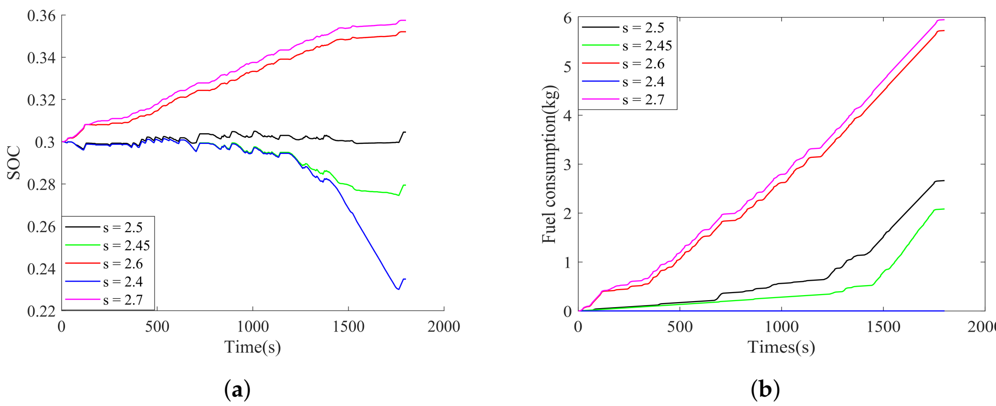

Figure 14. Simulation results of different equivalent factors. (**a**) Changes in the power battery SoC under different equivalent factors; (**b**) vehicle fuel consumption under different equivalent factors.

Conversely, when s decreases the car tends to use more electric power, resulting in a faster decrease in the SoC. In addition, in this paper, ECMS is based on the premise that the co-state variable $\lambda(t)$ remains constant. According to Equation (22), when the SoC changes too much, s is not constant, and the ECMS strategy cannot obtain the optimal solution. Therefore, when the SoC changes, an appropriate method is needed to make s to change adaptively.

4.2. MPC-ECMS Energy Management

According to the previous discussion, equivalent factors need to be adaptively adjusted. In the case of completing speed prediction, the combination of predictive speed and energy management can be achieved through the MPC framework, and the automatic adjustment of equivalent factors can be achieved through short-term planning. Combining any control method with the highly adaptable MPC control architecture can achieve real-time control. The fundamental premise of predictive control is to forecast the system's future output using the present model, the status of the system at hand, and upcoming control variables. Three elements comprise its management process: the rolling optimization, the feedback adjustment, and the forecast model. The MPC solution process is shown in Figure 15.

To achieve adaptive adjustment of the equivalent factors, the equivalent factors are first discretized with a suitable range at certain intervals. We use the multi-signal vehicle speed prediction model introduced in Section 3.3 to predict the speed in the next 5 s. The power generation range of the generator is from 0 to 285 kW, while the range of discretized equivalent factors is from 2.48 to 2.68. Then, the predicted velocity sequence is input into the control strategy by the prediction model. The control strategy calculates the required power sequence in 5 s based on the speed sequence. The best control sequence is calculated using PMP under different equivalent factors, and its fuel consumption and performance indicators are calculated accordingly. Since the performance indicator already considers the impact of the target SoC in the minimum principle, the calculated control variable enables the SoC satisfy the constraints. Finally, among all the corresponding relationships between the equivalent factors and the performance indicators, the equivalent factor that minimizes the performance indicator is selected as the designated equivalent factor s for the next moment. Meanwhile, the first control variable of the output sequence corresponding to the equivalent factor s is output as the output power of the range-extender at the next moment. The formula to solve the equivalent factor s is shown in Equation (27).

$$s = \arg\min(J) \tag{27}$$

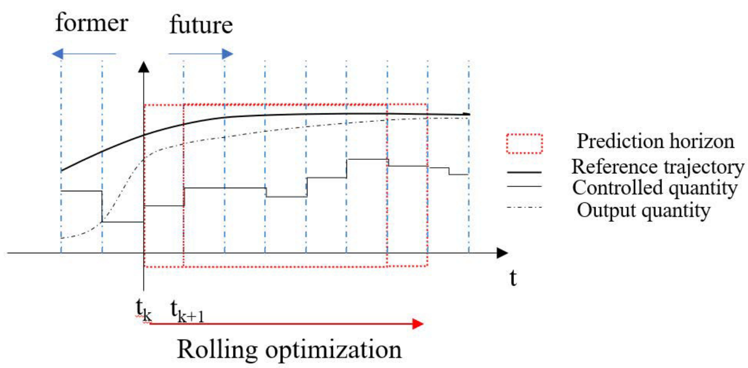

Figure 15. Principle of the MPC.

Although the control strategy can calculate the optimal control variable at each moment, there are a lot of fluctuations and inaccurate speed predictions in the cycling conditions, causing noise when calculating the required power of the whole vehicle. These noises cause an increase in fuel consumption. To eliminate the noise in the required power calculated by the control strategy without causing a large range of battery SoC changes, it is necessary to filter the required power of the range-extender calculated by the control strategy. This is because rapidly changing the engine power in a short time is not conducive to improving the engine's fuel economy. Experimental results show that this filtering method improves the fuel economy while having little effect on the SoC. The filtering method adopted here was first-order filtering, which is a simple control method with a good real-time performance and very beneficial for eliminating power noise. The discrete formula of the first-order filtering is shown as Equation (28).

$$Y(n) = aU(n) + (1-a)Y(n-1) \tag{28}$$

where Y represents the required power of the range-extender after filtering, n represents the time step, U is the power calculated by the control strategy,and a is a coefficient.

Here, we mainly focus on the multi-signal LSTM vehicle speed prediction MPC-ECMS (multi-signal-LSTM-MPC-ECMS). We set the initial SoC to 0.3 for the conducted simulation, and compared the control effect of the proposed strategy with the MPC-ECMS under SVM vehicle speed prediction (SVM-MPC-ECMS), dynamic programming (DP), ECMS ($s = 2.5$) and power-following control strategy. Each control strategy used the same coefficient for filtering, and the comparison before and after power noise filtering is shown in Figure 16.In the figure, the red line indicates the signal change after filtering and the blue line indicates the signal change before filtering. The final SoC and fuel consumption before and after filtering for each control strategy are shown in Table 4. When the entire working condition is in the pure electric drive mode, the final SoC is 0.2349. The experimental results under various control strategies show that the SoC is still within the allowable range after filtering. A greater reduction in fuel consumption is achieved relative to the reduction in SoC.

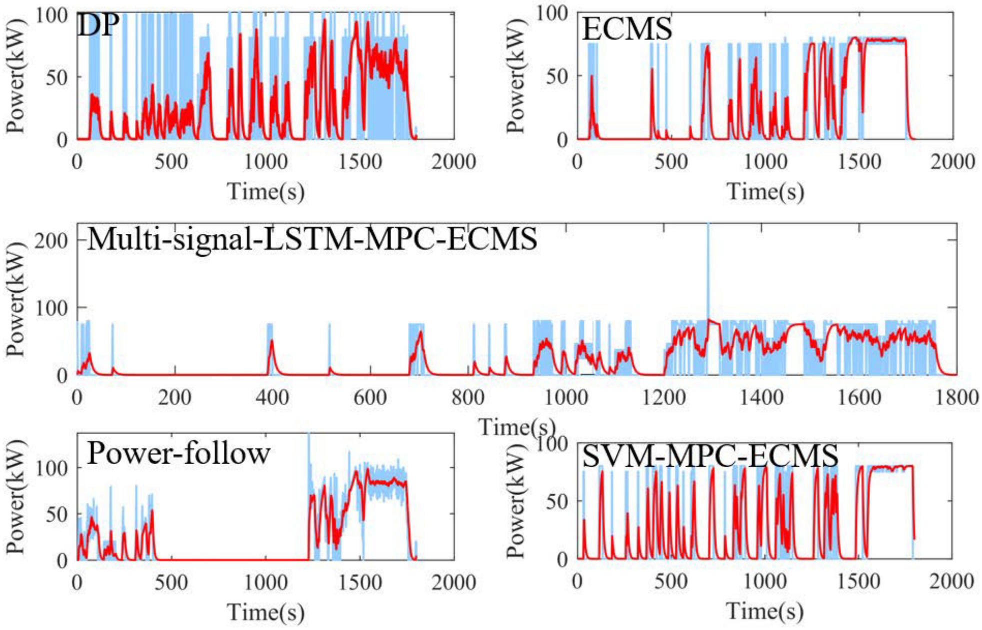

Figure 16. Comparison of the output power before and after filtering for each control strategy.

Table 4. Performance comparison before and after filtering under the different control strategies.

Control Strategy	SoC		Fuel Consumption (kg)	
	Pre-Filter	**After-Filter**	**Pre-Filter**	**After-Filter**
DP	0.2938	0.2902	2.9637	2.536
ECMS ($s = 2.5$)	0.308	0.3045	3.112	2.663
Multi-signal-LSTM-MPC-ECMS	0.3031	0.2976	3.02	2.627
Power-follow	0.306	0.3052	3.103	2.902
SVM-MPC-ECMS	0.3013	0.2985	3.505	3.115

As shown in Figure 17, the ordinate is $\Delta SOC/C_{fuel}$, ΔSOC is the difference between the final SoC under this control strategy and the final SoC under the pure electric drive mode, and C_{fuel} is the total fuel consumption under this control strategy. The results show that SoC variation under unit fuel consumption after filtering is significant, so filtering is helpful for fuel saving.

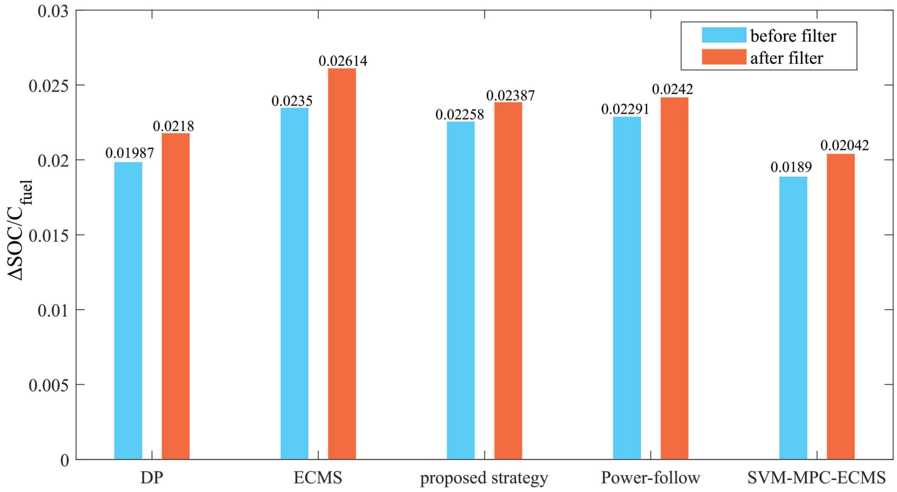

Figure 17. Performance comparison chart before and after output power filtering for each control strategy.

4.3. HIL Simulation Experiment

In order to validate the precision and real-time effectiveness of the control strategy, a HIL simulation experimental platform was built to simulate the multi-signal LSTM-MPC-ECMS control strategy. A schematic diagram of the HIL is shown in Figure 18. The HIL simulation experimental platform equipment mainly consists of an upper computer, a MicroAutoBox controller, and a SCALEXIO real-time simulation hardware system. The upper computer is responsible for monitoring the entire simulation process and saving the results, the controller is responsible for simulating the electronic control unit, making decisions according to the control strategy, and the real-time simulation hardware system is used to simulate the behaviour of the whole vehicle, providing a complete vehicle environment for HCU. SCALEXIO and AUTOBOX are connected to the upper computer through network cables, and the harness interface connects SCALEXIO to the expansion version. SCALEXIO is connected to the expansion board of AUTOBOX through the CAN high/low lines for signal transmission.

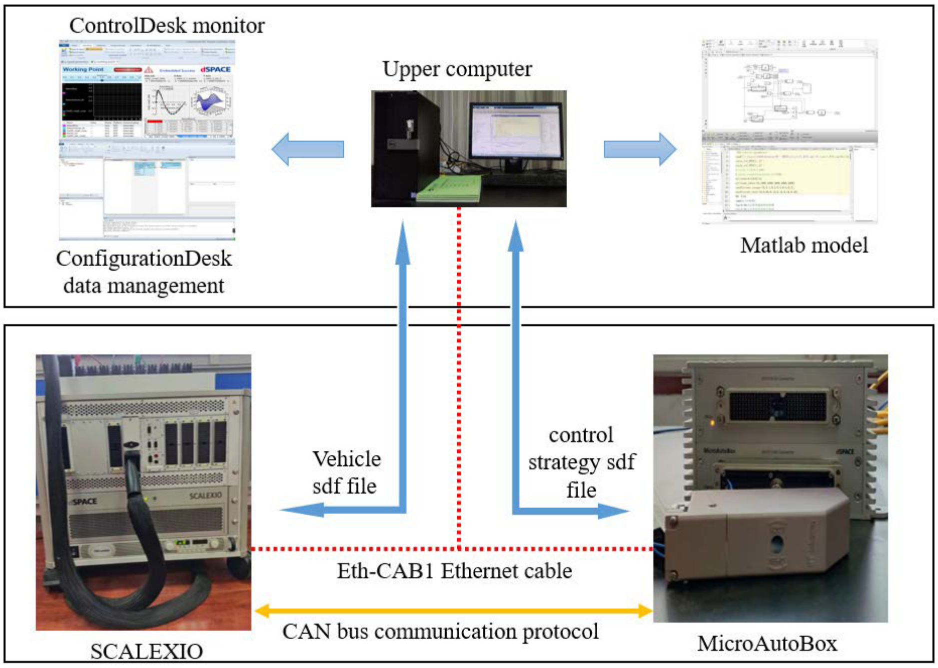

Figure 18. Schematic of the hardware-in-the-loop simulation.

5. Results and Discussion

After the HIL simulation, the results of the proposed strategy are compared with other control strategies using WTVC as the cycle condition; the initial SoC was 0.3. The change in the battery SoC and the fuel consumption under various control strategies are shown in Figure 19. We found that the other control strategies result in relatively a stable battery SoC, except for the DP and SVM-MPC-ECMS control strategies. Because the DP algorithm only considers the final SoC value, it does not pay attention to the changes in the SoC during the process. The vehicle speed prediction of the SVM-MPC-ECMS is worse than the proposed control strategy. Among all the control strategies, the DP is the least fuel consumptive because it is the theoretical optimal solution; however, the DP is difficult to implement in the actual driving process, making it commonly used as a theoretical reference for the economy of other control strategies. From Figure 19b, it can be seen that the proposed strategy is the closest to the DP algorithm, while MPC-ECMS under LSTM multi-signal vehicle speed prediction fuel consumption was reduced by 1.352% relative to the ECMS ($s = 2.5$) strategy, 9.476% relative to the power-following control strategy, and a decrease of 15.7% relative to the SVM-MPC-ECMS. Both multi-signal-LSTM-MPC-ECMS and SVM-MPC-ECMS are MPC-ECMS control strategies. The difference between them is their method of predicting vehicle speed. Figure 20 shows the economic changes of these two control strategies compared to the other control strategies. The numbers represent the ratio of fuel savings compared to the other control strategies. We found that the multi-signal-LSTM-MPC-ECMS control strategy is more economical than the SVM-MPC-ECMS. The reason is that in the vehicle speed prediction part, the Multi-signal-LSTM prediction achieves higher accuracy, which shows that the prediction accuracy of the prediction part directly affects the control effect of the MPC-ECMS control strategy.

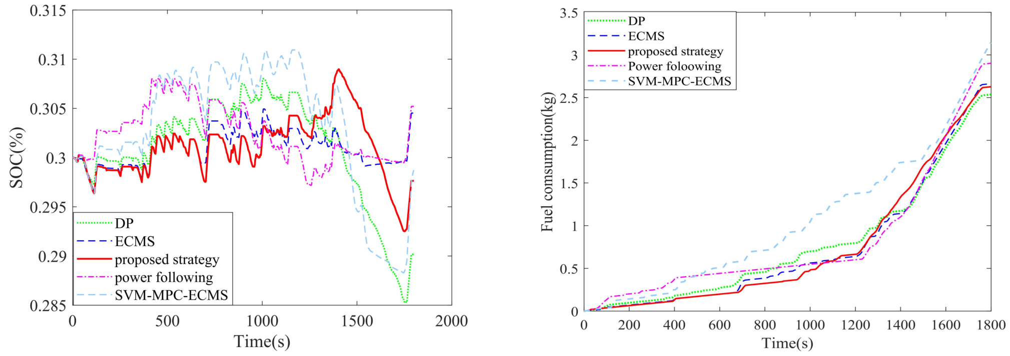

(**a**) (**b**)

Figure 19. Graph of changes under various control strategy SOCs. (**a**) Comparison of the changes in SoC for different control strategies; (**b**) the fuel consumption of the different control strategies.

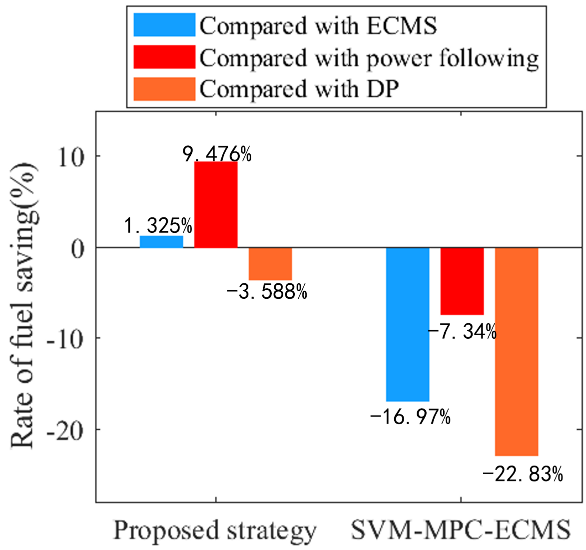

Figure 20. Comparison of different MPC-ECMS control strategies in terms of economic efficiency.

Compared with rule-based control strategies, such as power-following, MPC-ECMS control strategies can provide better control in the time domain. Compared with the ECMS, the MPC-ECMS can adapt to various changing working conditions, and this fully reflects the advantage of the MPC-ECMS control strategy to change the generator output power in real-time. The change in the MPC-ECMS equivalent factor under LSTM multi-signal vehicle speed prediction is shown in Figure 21. The diagram shows that the MPC-ECMS energy management strategy can adapt to different working conditions by constantly adjusting the equivalence factor.

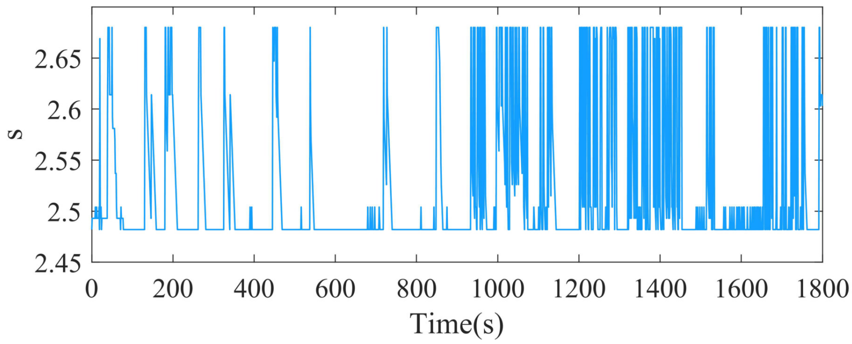

Figure 21. Proposed control strategy equivalent factor change chart.

Figure 22 shows the working points of the engine and generator under various control strategies; the dotted line in the figure is the optimal working curve of the range-extender. The engine and generator jointly influence the optimal working curve of a range-extender; therefore, the optimal working speed and torque should be calculated based on this curve. From the distribution diagram of the working points, we find that most of the working points of the MPC-ECMS control strategy are concentrated near the optimal curve, whether it is the MPC-ECMS method proposed in this article or the SVM-MPC-ECMS, in which the points that are not on the optimal curve are mainly the operating points in the speed transition stage. It can be seen that improving the prediction accuracy and extending the prediction time domain in order to optimize over a longer period of time can enable the range-extender to work nearer the optimal curve. We believe that improving the prediction accuracy while extending the prediction time domain will not only allow control strategies to have longer planning time and greater control accuracy, but also make full use of the high-efficiency range of the engine, reducing the rapid changes in speed and torque in a short time, and thereby improve the overall fuel efficiency. However, the optimal working curve of the range-extender is significantly influenced by the generator's efficiency, resulting in a difference between the optimal operating curves of the range-extender and the engine. This difference can be seen from the fuel consumption and working point distribution of engines with different control strategies.

The control strategy proposed in this paper calculates the demand power sequence in the future by predicting the vehicle speed in the future time domain, facilitating the controller to plan better. The experimental results show that the fuel consumption of the whole vehicle decreases significantly under this control strategy, and the engine works in the efficient zone most of the time. This control strategy is applicable to many types of vehicles. In addition, the study of speed prediction can be applied to the vehicle following conditions by predicting the speed of the preceding vehicle to predict the operating condition of the main vehicle.

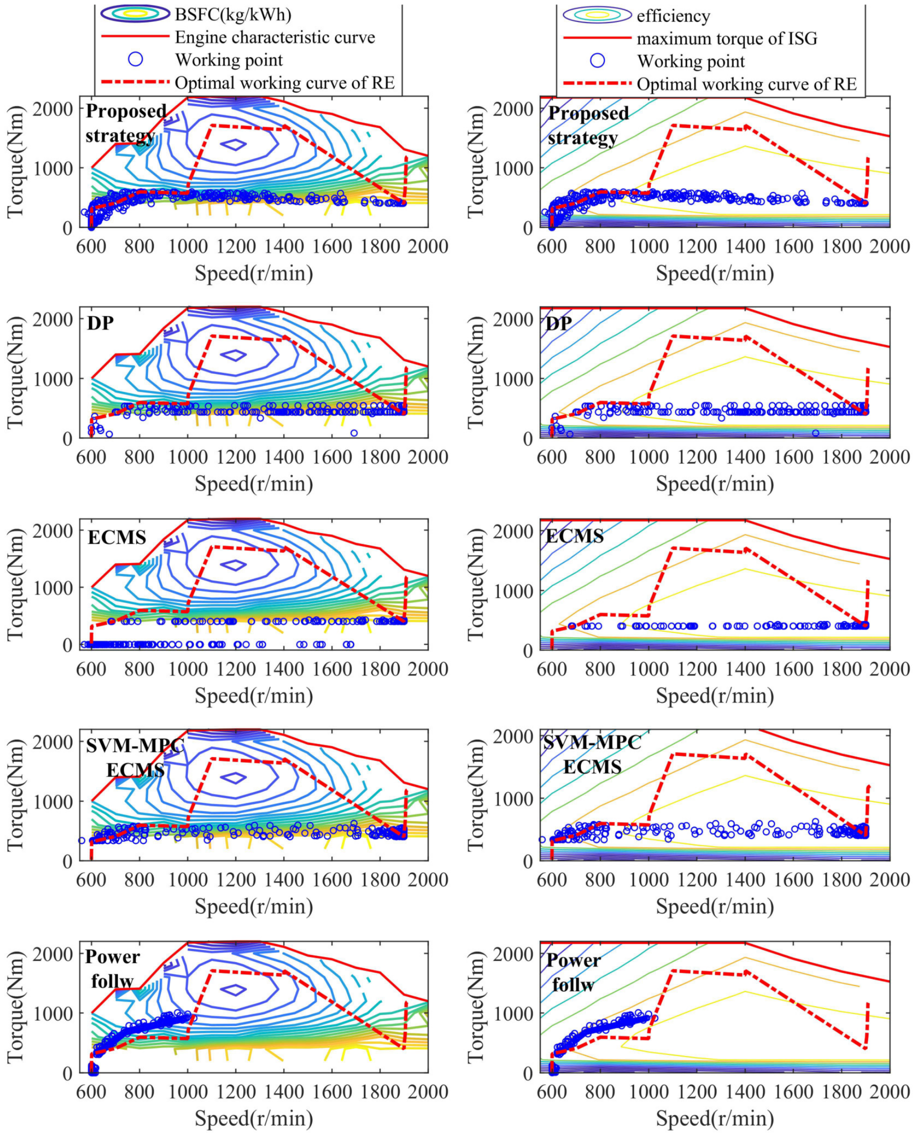

Figure 22. Distribution of the engine and generator operating points for the different control strategies.

6. Conclusions

In this paper, the multi-signal LSTM speed prediction model is combined with MPC-ECMS for energy management to improve the fuel economy.

Firstly, the proposed vehicle speed prediction method has a better prediction accuracy when compared to the SVM vehicle speed prediction method. The LSTM-based vehicle speed prediction model can train a large amount of training data, but the prediction speed will be slower when the SVM training data increases. SVM parameter adjustment will also have a great impact on the prediction effect.

Secondly, the control effect of the MPC-ECMS based on speed prediction is closely related to the accuracy of prediction; therefore, improving the prediction accuracy is beneficial to expand the prediction time domain, allowing the control strategy to make plans for longer periods of time. A prediction time domain that is too short is not only difficult to plan for in time, but it cannot take full advantage of the efficient area of the range-extender. Compared with other LSTM-based speed prediction models, the proposed multi-signal LSTM speed prediction model considers the influence of multiple other vehicle signals on the future speed, which is more conducive to improving the prediction accuracy.

Finally, although the prediction model used in this article can predict vehicle speed with high accuracy, actual driving environments still contain complex operating conditions, such as sharp changes in torque demand during climbing. Therefore, in future work we consider torque prediction, enabling a more accurate calculation of the demand power by variations in torque, thus resulting in greater adaptivity of the equivalence factor.

Author Contributions: Software, methodology ,validation, writing—original draft preparation, visualization, L.L.; writing—review and editing, supervision, project administration, funding acquisition, H.Z.; investigation, X.L.; data curation, C.S.; formal analysis , X.Z.; conceptualization, H.Y. All authors have read and agreed to the published version of the manuscript.

Funding: This work was supported by the Key Research and Development Plan of Shandong Province of China (No. 2018GGX105004) and Qingdao Civi Science and Technology Plan (No. 19-6-1-88-nsh).

Institutional Review Board Statement: Not applicable.

Informed Consent Statement: Not applicable.

Data Availability Statement: The data presented in this study are available on request from the corresponding author.

Acknowledgments: The authors thank the editors and the anonymous reviewers for their constructive feedback and valuable advice.

Conflicts of Interest: The authors declare no conflicts of interest.

Abbreviations

The following abbreviations are used in this manuscript:

LSTM	Long short-term memory neural networks
MPC	Model predictive control
ECMS	Equivalent fuel consumption minimum strategy
SVM	Support vector machine
SVR	Support vector regression
SoC	State of charge
DP	Dynamic programming
WTVC	World transient vehicle cycle
HIL	Hardware-in-the-loop

References

1. Zhao, H.; Mu, L.; Li, Y.; Qiu, J.; Sun, C.; Liu, X. Unregulated Emissions from Natural Gas Taxi Based on IVE Model. *Atmosphere* **2021**, *12*, 478. [CrossRef]
2. Liu, C.; Wang, Y.; Wang, L.; Chen, Z. Load-adaptive real-time energy management strategy for battery/ultracapacitor hybrid energy storage system using dynamic programming optimization. *J. Power Sources* **2019**, *438*, 227024. [CrossRef]
3. Zhang, N.; Ma, X.; Jin, L. Energy management for parallel HEV based on PMP algorithm. In Proceedings of the IEEE 2017 2nd International Conference on Robotics and Automation Engineering (ICRAE), Shanghai, China, 29–31 December 2017; pp. 177–182.
4. Musardo, C.; Rizzoni, G.; Guezennec, Y.; Staccia, B. A-ECMS: An adaptive algorithm for hybrid electric vehicle energy management. *Eur. J. Control* **2005**, *11*, 509–524. [CrossRef]
5. Yuan, Z.; Teng, L.; Fengchun, S.; Peng, H. Comparative study of dynamic programming and Pontryagin's minimum principle on energy management for a parallel hybrid electric vehicle. *Energies* **2013**, *6*, 2305–2318. [CrossRef]
6. Zhang, H.; Fu, L.; Song, J.; Yang, Q. Power energy management and control strategy study for extended-range auxiliary power unit. *Energy Procedia* **2016**, *104*, 32–37. [CrossRef]
7. Chen, B.C.; Wu, Y.Y.; Tsai, H.C. Design and analysis of power management strategy for range extended electric vehicle using dynamic programming. *Appl. Energy* **2014**, *113*, 1764–1774. [CrossRef]
8. Pan, C.; Liang, Y.; Chen, L.; Chen, L. Optimal control for hybrid energy storage electric vehicle to achieve energy saving using dynamic programming approach. *Energies* **2019**, *12*, 588. [CrossRef]
9. Rezaei, A.; Burl, J.B.; Zhou, B. Estimation of the ECMS equivalent factor bounds for hybrid electric vehicles. *IEEE Trans. Control. Syst. Technol.* **2017**, *26*, 2198–2205. [CrossRef]
10. Yu, X.; Lin, C.; Tian, Y.; Zhao, M.; Liu, H.; Xie, P.; Zhang, J. Real-time and hierarchical energy management-control framework for electric vehicles with dual-motor powertrain system. *Energy* **2023**, *272*, 127112. [CrossRef]
11. Shen, P.; Zhao, Z.; Zhan, X.; Li, J.; Guo, Q. Optimal energy management strategy for a plug-in hybrid electric commercial vehicle based on velocity prediction. *Energy* **2018**, *155*, 838–852. [CrossRef]

12. Wang, W.; Guo, X.; Yang, C.; Zhang, Y.; Zhao, Y.; Huang, D.; Xiang, C. A multi-objective optimization energy management strategy for power split HEV based on velocity prediction. *Energy* **2022**, *238*, 121714. [CrossRef]
13. Xing, J.; Chu, L.; Hou, Z.; Sun, W.; Zhang, Y. Energy Management Strategy Based on a Novel Speed Prediction Method. *Sensors* **2021**, *21*, 8273. [CrossRef]
14. Chen, R.; Yang, C.; Han, L.; Wang, W.; Ma, Y.; Xiang, C. Power reserve predictive control strategy for hybrid electric vehicle using recognition-based long short-term memory network. *J. Power Sources* **2022**, *520*, 230865. [CrossRef]
15. Han, J.; Shu, H.; Tang, X.; Lin, X.; Liu, C.; Hu, X. Predictive energy management for plug-in hybrid electric vehicles considering electric motor thermal dynamics. *Energy Convers. Manag.* **2022**, *251*, 115022. [CrossRef]
16. Lin, X.; Wu, J.; Wei, Y. An ensemble learning velocity prediction-based energy management strategy for a plug-in hybrid electric vehicle considering driving pattern adaptive reference SOC. *Energy* **2021**, *234*, 121308. [CrossRef]
17. Ritter, A.; Widmer, F.; Duhr, P.; Onder, C.H. Long-term stochastic model predictive control for the energy management of hybrid electric vehicles using Pontryagin's minimum principle and scenario-based optimization. *Appl. Energy* **2022**, *322*, 119192. [CrossRef]
18. Li, M.; He, H.; Feng, L.; Chen, Y.; Yan, M. Hierarchical predictive energy management of hybrid electric buses based on driver information. *J. Clean. Prod.* **2020**, *269*, 122374. [CrossRef]
19. Wei, C.; Chen, Y.; Li, X.; Lin, X. Integrating intelligent driving pattern recognition with adaptive energy management strategy for extender range electric logistics vehicle. *Energy* **2022**, *247*, 123478. [CrossRef]
20. Chen, Z.; Gu, H.; Shen, S.; Shen, J. Energy management strategy for power-split plug-in hybrid electric vehicle based on MPC and double Q-learning. *Energy* **2022**, *245*, 123182. [CrossRef]
21. Lin, X.; Zhang, J.; Su, L. A trip distance adaptive real-time optimal energy management strategy for a plug-in hybrid vehicle integrated driving condition prediction. *J. Energy Storage* **2022**, *52*, 105055. [CrossRef]
22. Zhao, Z.; Xun, J.; Wan, X.; Yu, R. Mpc based hybrid electric vehicles energy management strategy. *IFAC-PapersOnLine* **2021**, *54*, 370–375. [CrossRef]
23. Wang, Y.; Zhang, Y.; Zhang, C.; Zhou, J.; Hu, D.; Yi, F.; Fan, Z.; Zeng, T. Genetic algorithm-based fuzzy optimization of energy management strategy for fuel cell vehicles considering driving cycles recognition. *Energy* **2023**, *263*, 126112. [CrossRef]
24. Zhou, Y.; Ravey, A.; Péra, M.C. Multi-mode predictive energy management for fuel cell hybrid electric vehicles using Markov driving pattern recognizer. *Appl. Energy* **2020**, *258*, 114057. [CrossRef]
25. Türker, E.; Bulut, E.; Kahraman, A.; Çakıcı, M.; Öztürk, F. Estimation of Energy Management Strategy Using Neural-Network-Based Surrogate Model for Range Extended Vehicle. *Appl. Sci.* **2022**, *12*, 12935. [CrossRef]
26. Al-Saadi, Z.; Phan Van, D.; Moradi Amani, A.; Fayyazi, M.; Sadat Sajjadi, S.; Ba Pham, D.; Jazar, R.; Khayyam, H. Intelligent Driver Assistance and Energy Management Systems of Hybrid Electric Autonomous Vehicles. *Sustainability* **2022**, *14*, 9378. [CrossRef]
27. Wang, H.; Huang, Y.; Khajepour, A.; Song, Q. Model predictive control-based energy management strategy for a series hybrid electric tracked vehicle. *Appl. Energy* **2016**, *182*, 105–114. [CrossRef]
28. Mu, L.; Zhao, H.; Li, Y.; Liu, X.; Qiu, J.; Sun, C. Traffic flow statistics method based on deep learning and multi-feature fusion. *CMES Comput. Model. Eng. Sci.* **2021**, *129*, 465–483. [CrossRef]
29. Hong, J.; Wang, Z.; Qu, C.; Zhou, Y.; Shan, T.; Zhang, J.; Hou, Y. Investigation on overcharge-caused thermal runaway of lithium-ion batteries in real-world electric vehicles. *Appl. Energy* **2022**, *321*, 119229. [CrossRef]
30. Hong, J.; Zhang, H.; Xu, X. Thermal fault prognosis of lithium-ion batteries in real-world electric vehicles using self-attention mechanism networks. *Appl. Therm. Eng.* **2023**, *226*, 120304. [CrossRef]
31. Sun, X.; Fu, J.; Yang, H.; Xie, M.; Liu, J. An energy management strategy for plug-in hybrid electric vehicles based on deep learning and improved model predictive control. *Energy* **2023**, *269*, 126772. [CrossRef]